Relating the Morphology of Poly(*p*-phenylene vinylene)/ Methanofullerene Blends to Solar-Cell Performance**

By *Jeroen K. J. van Duren*, *Xiaoniu Yang*, *Joachim Loos*, *Corrie W. T. Bulle-Lieuwma*, *Alexander B. Sieval*, *Jan C. Hummelen*, and *René A. J. Janssen**

The performance of bulk-heterojunction solar cells based on a phase-separated mixture of donor and acceptor materials is known to be critically dependent on the morphology of the active layer. Here we use a combination of techniques to resolve the morphology of spin cast films of poly(*p*-phenylene vinylene)/methanofullerene blends in three dimensions on a nanometer scale and relate the results to the performance of the corresponding solar cells. Atomic force microscopy (AFM), transmission electron microscopy (TEM), and depth profiling using dynamic time-of-flight secondary ion mass spectrometry (TOF-SIMS) clearly show that for the two materials used in this study, 1-(3-methoxycarbonyl)propyl-1-phenyl-[6,6]-methanofullerene (PCBM) and poly[2-methoxy-5-(3′,7′-dimethyloctyloxy)-1,4-phenylene vinylene] (MDMO-PPV), phase separation is not observed up to 50 wt.-% PCBM. Nanoscale phase separation throughout the film sets in for concentrations of more than 67 wt.-% PCBM, to give domains of rather pure PCBM in a homogenous matrix of 50:50 wt.-% MDMO-PPV/PCBM. Electrical characterization, under illumination and in the dark, of the corresponding photovoltaic devices revealed a strong increase of power conversion efficiency when the phase-separated network develops, with a sharp increase of the photocurrent and fill factor between 50 and 67 wt.-% PCBM. As the phase separation sets in, enhanced electron transport and a reduction of bimolecular charge recombination provide the conditions for improved performance. The results are interpreted in terms of a model that proposes a hierarchical build up of two cooperative interpenetrating networks at different length scales.

1. Introduction

In bulk-heterojunction organic solar cells, two different organic materials with donor and acceptor properties, respectively, are mixed to create a composite material that is capable of generating charges under illumination, followed by transporting and collecting these photogenerated charges into an external circuit.[1,2] Promising power conversion efficiencies of > 3 % have recently been reported for solar cells based on this approach utilizing conjugated polymers as a donor and fullerene derivatives as an acceptor.[3,4] In these cells a sub-picosecond photoinduced charge transfer[5,6] ensures efficient charge generation, while the collection of charges is facilitated by a slow recombination that extends into the millisecond domain.[7,8] It has been shown that both the conditions for processing of these mixtures from solution[4,9,10] and post-production treatment[11,12] can have a large influence on the performance of these devices, because they affect the morphology and phase separation of the active layer dramatically. The generation, transport, and collection of the charges are strongly influenced by the characteristic dimensions of the phase separation of the photoactive film and the presence of percolation pathways.

Although some useful insights on the interplay between morphology and solar-cell performance have been obtained,[4,9,13] a comprehensive understanding is lacking and so far no systematic study has been performed in which morphology and performance have been studied in detail for polymer/fullerene blends. On the other hand, detailed studies on the relation between morphology and performance have been described for photoactive layers based on donor and acceptor polymer blends.[14,15] In this paper we specifically consider the phase separation and performance of solar cells based on poly[2-methoxy-5-(3′,7′-dimethyloctyloxy)-1,4-phenylene vinylene] (MDMO-PPV) as a donor and 1-(3-methoxycarbonyl)propyl-1-phenyl-[6,6]-methanofullerene (PCBM) as an acceptor (Fig. 1). Since the breakthrough discovery by the Linz group that solar cells with a power conversion efficiency of 2.5 % under AM 1.5 conditions can be obtained using chlorobenzene as

[*] Prof. R. A. J. Janssen, Dr. J. K. J. van Duren
Molecular Materials and Nanosystems
Eindhoven University of Technology
P.O. Box 513, NL-5600 MB Eindhoven (The Netherlands)
E-mail: r.a.j.janssen@tue.nl
Dr. X. Yang, Dr. J. Loos
Dutch Polymer Institute and Group Polymer Physics
Eindhoven University of Technology
P.O. Box 513, NL-5600 MB Eindhoven (The Netherlands)
Dr. C. W. T. Bulle-Lieuwma
Philips CFT
Prof. Holstlaan 4, NL-5656 AA Eindhoven (The Netherlands)
Dr. A. B. Sieval, Prof. J. C. Hummelen
Molecular Electronics, MSC plus and Biomade Technology
University of Groningen
Nijenborgh 4, NL-9747 AG Groningen (The Netherlands)

[**] These investigations were financially supported by the Dutch Ministries of EZ, O&W, and VROM through the EET program (EETK97115). The work of X. Y. and J. L. forms part of the research program of the Dutch Polymer Institute (DPI). We would like to acknowledge Philips for a generous gift of MDMO-PPV, Dr. M. T. Rispens for the synthesis of PCBM, Dr. M. M. Koetse (TNO) for the IPCE measurements, and Dr. S. C. J. Meskers for helpful discussions.

 DOI: 10.1002/adfm.200305049

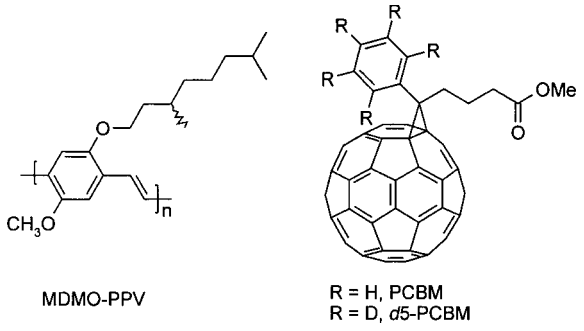

Figure 1. Molecular structures of materials used.

a solvent for spin-coating,[9] this combination of materials has become the subject of detailed studies. In general the performance of donor–acceptor bulk-heterojunction solar cells relies on an intricate balance between light absorption, charge generation, transport, and collection of charges. In these cells, the polymer absorbs most of the light, because C_{60} derivatives such as PCBM have an almost negligible absorption coefficient in the visible region. It is therefore somewhat surprising that the most efficient solar cells based on MDMO-PPV and PCBM require a high content (80 wt.-%) of the latter.[9] This point became even more startling when it turned out recently that the charge-carrier mobility for electrons in PCBM is more than three orders of magnitude larger than that for the holes in pure MDMO-PPV.[16] This poses an intriguing and fundamental question to the future design of more efficient plastic solar cells: Why do the cells require 80 wt.-% of a material that hardly contributes to light absorption and transports charges more efficiently? Intuitively one would reason that increasing the concentration of MDMO-PPV would be beneficial, for absorption and the number of possible charge percolation pathways, but apparently it is not. As outlined above, it has been recognized that morphology and molecular organization on the nanometer scale is a key issue in this respect.

To obtain a deeper insight in the relation between morphology and performance of polymer/fullerene bulk-heterojunction solar cells, both have to be characterized. However, few techniques are available where the morphology of organic blends can be determined in all three dimensions on a nanometer scale. One way to achieve this goal is by combining different methods. Here we present a comprehensive study on solar cells made with varying weight percentages of PCBM in MDMO-PPV in the active layer. The composite films have been investigated with atomic force microscopy (AFM), transmission electron microscopy (TEM), dynamic time-of-flight secondary ion mass spectrometry (TOF-SIMS), and time-correlated single photon counting to reveal the morphology of these composites. The same films have also been incorporated into devices and have been fully characterized in the dark, under illumination, and for their monochromatic spectral response. By combining the morphological and electro-optical characterization, we have been able to rationalize some of the intriguing issues described above.

2. Results and Discussion

2.1. Atomic Force Microscopy

Figure 2 shows the height and corresponding phase images obtained by atomic force microscopy (AFM) for composite MDMO-PPV/PCBM films (~100 nm) for four different compositions. The height images are similar to those previously reported.[13] To match the conditions used for device preparation and to exclude any possible influence of the substrate, all films in this study were spin cast from chlorobenzene on indium tin

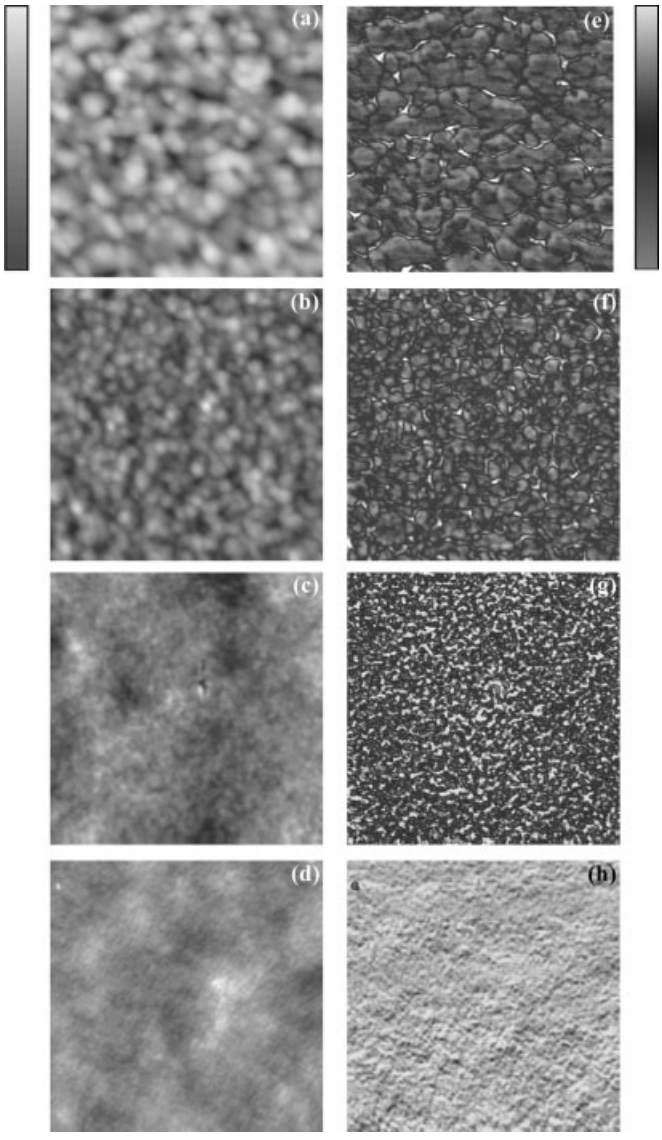

Figure 2. The AFM height (a–d) and simultaneously taken phase (e–h) images of the MDMO-PPV/PCBM composite films of 90 (a,e), 80 (b,f), 67 (c,g), and 50 wt.-% PCBM (d,h). Height bar (maximum peak-to-valley) represents 20 nm (a), 10 nm (b), 3 nm (c), and 3 nm (d). The size of the images is 2.0 μm × 2.0 μm.

ADVANCED FUNCTIONAL MATERIALS

oxide (ITO)-covered glass substrates covered an additional layer of a transparent conducting polymer (poly(3,4-ethylenedioxythiophene)–poly(styrene sulfonic acid) (PEDOT–PSS)). Apart from the images shown in Figure 2, compositions of 0, 33, 50, 67, 75, 80, 90, and 100 wt.-% PCBM in MDMO-PPV have been studied with AFM. The height images reveal extremely smooth surfaces for the pure films and for the blends with a PCBM concentration of 2–50 wt.-% (peak-to-valley roughness of 3 nm and root-mean-square (RMS) values of 0.4 nm for 2.0 μm × 2.0 μm). The surface becomes increasingly uneven for 67–90 wt.-% PCBM (peak-to-valley roughness of 3–22 nm and RMS values of 0.4–3.3 nm for 2.0 μm × 2.0 μm) and a reproducible phase contrast appears. Separate domains of one phase in a matrix of another phase can easily be recognized at these higher concentrations of PCBM. X-ray photoelectron spectroscopy (XPS) measurements (not shown) on the 80 wt.-% PCBM composite film confirmed that both components are present at the top of the film. The domain size increases from 40–65 nm for 67 wt.-% to 110–200 nm for 90 wt.-% PCBM. For 80 wt.-% PCBM composite films, a gradual but small increase in domain size from 60–80 nm to 100–130 nm was observed when the film thickness was increased in steps from 65 to 270 nm.

2.2. Transmission Electron Microscopy

Where AFM provides surface characteristics, transmission electron microscopy (TEM) can be used for lateral resolution in the bulk of the film.[13] For TEM, the films were either floated with water from the glass/ITO/PEDOT–PSS substrates or mechanically removed and subsequently transferred as a free-standing film to a Cu grid. Composites varying from 0, to 20, 40, 60, 75, 80, 90, and 100 wt.-% PCBM were investigated. The TEM images (Fig. 3) show that bulk characteristics are similar to those at the surface. Up to 50 wt.-% PCBM, no contrast in TEM images is observed. Although this can be interpreted in terms of an absence of phase separation, it might also mean that phase separation occurs in tiny domains that are small compared to the film thickness, resulting in no observable contrast. Yet, it seems that the matrix consists of a fairly homogenous composite with roughly 50 wt.-% MDMO-PPV and 50 wt.-% PCBM. Again, phase separation is setting in somewhere between 60 and 75 wt.-% PCBM. The dark regions are PCBM rich, as can be concluded from the higher density for pure spin-cast films of PCBM (1500 kg m^{-3}) compared to that of MDMO-PPV (910 kg m^{-3}).[17] From TEM, we conclude that MDMO-PPV can contain at least 50 wt.-% PCBM before detectable phase separation sets in.

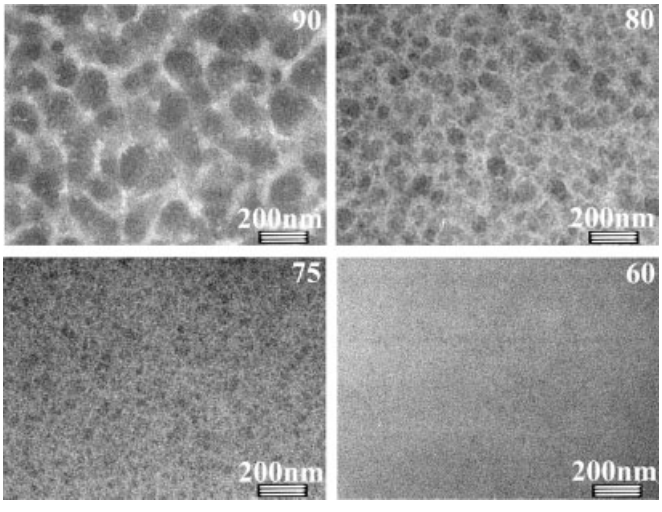

Figure 3. TEM images of MDMO-PPV/PCBM blends with different weight percentages of PCBM as indicated in the upper right corner.

2.3. Depth Profiling with Time-of-Flight Secondary Ion Mass Spectrometry (TOF-SIMS)

Determining a distribution in depth of an organic component in a composite film where both components do not have a distinctive element can be accomplished by labeling one of the two components. Deuterium labeling in combination with dynamic SIMS has proven its usefulness for this purpose.[18–21] To enable recording depth profiles of PCBM in the photoactive films with MDMO-PPV, a deuterated derivative (d5-PCBM, Fig. 1) has been synthesized that carries five deuterium atoms on the phenyl ring. Using dynamic TOF-SIMS, deuterium-related mass fragments can be used to measure a concentration depth profile of d5-PCBM in the photoactive films. We note that AFM, TEM, and solar-cell characteristics demonstrated that the morphology and performance of MDMO-PPV/d5-PCBM blends was identical to that of MDMO-PPV/PCBM composites. Various MDMO-PPV/d5-PCBM (0, 20, 40, 60, 75, 80, 90, and 100 wt.-% d5-PCBM) films (~100 nm) spin-cast from chlorobenzene on glass/ITO/PEDOT–PSS have been investigated with dynamic TOF-SIMS. Although a single secondary ion, specific for the deuterium label, would be enough for depth profiling, several secondary ions specific to the label were observed and used as such. Hence, apart from D, also CD, CHD, OD, and C_2D were monitored. CHD and OD obviously result from deuterium transfer during sputtering, just as proton transfer, commonly observed in dynamic TOF-SIMS for organic samples.[22] As shown in Figure 4 for 80 wt.-%, d5-PCBM is present all over depth. The same result has been observed for all other compositions with a clear increase in counts for the deuterium-related mass fragments going from 0 to 100 wt.-% d5-PCBM in the film. The first region with the initial increase in yields is attributed, at least in part, to the pre-equilibrium regime. For 80 wt.-% d5-PCBM, we found that d5-PCBM was present at all depths, regardless of the film thickness when it was varied from 65 to 270 nm.

To study the morphology at different depths, six craters were sputtered at depths ranging from 10 to 90 nm in the ~100 nm 80 wt.-% MDMO-PPV/d5-PCBM film. When studied with AFM, the bottoms of these craters (Fig. 4) showed that the lateral phase distribution present at the top surface is present all over depth, although with slightly increasing domain size.

The TOF-SIMS results show that no spontaneous stratification occurs,[23] consistent with our previous conclusion for com-

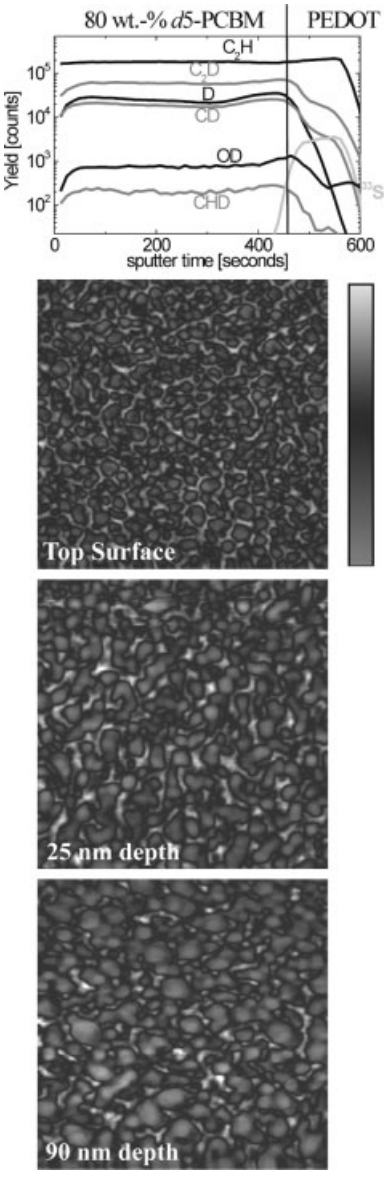

Figure 4. Above: Depth profile of an 80 wt.-% d5-PCBM blend with MDMO-PPV as measured with dynamic TOF-SIMS. Several deuterium-related negative ions are depicted versus sputter time (depth). Below: 2.0 μm × 2.0 μm AFM phase images at the top surface and on two crater bottoms for the 80 wt.-% d5-PCBM blend.

posites of MDMO-PPV with an iodinated PCBM derivative studied by cryogenic Rutherford back scattering.[24] In addition, TEM images of a cross-section made with cryo-ultramicrotomy of a spin-cast film of an MDMO-PPV/PCBM composite on top of a poly(ethylene terephthalate) (PET) substrate showed PCBM-rich domains all over depth.[13]

2.4. Fluorescence Spectroscopy

The optical absorption spectra of films spin-cast on glass from chlorobenzene with concentrations varying from 0 to 100 wt.-% PCBM (0, 2, 5, 10, 14, 20, 30, 40, 50, 60, 67, 75, 80, 85, 90, 95, and 100 wt.-%) show the expected variation in composition. Savenije et al. recently showed that the spectra of such composite films correspond to a linear superposition of the spectra of the individual compounds with the same concentration PCBM in the film as in the solution used for spin-casting these films.[25]

When the composite films are illuminated with light of 655 nm, i.e., outside the absorption spectrum of MDMO-PPV, such that only PCBM is photoexcited, the photoluminescence (PL) spectra clearly show the presence of a weak fullerene fluorescence with a maximum at ~722 nm for films with 75–100 wt.-% PCBM, decreasing further in intensity with decreasing amount of PCBM. For blends with 67 wt.-% PCBM or less, fullerene emission can no longer be observed under these conditions.

When the excitation wavelength is shifted to 500 or 400 nm, where both MDMO-PPV and PCBM absorb light, the PCBM emission can again be detected down to 75 wt.-% (Fig. 5). In addition to the fullerene emission around 722 nm, a signal centered at ~580 nm can be seen up to at least 85 wt.-% PCBM. It must be noted that already at 2 wt.-% of PCBM virtually all MDMO-PPV fluorescence is quenched.[5] Hence, the ~580 nm

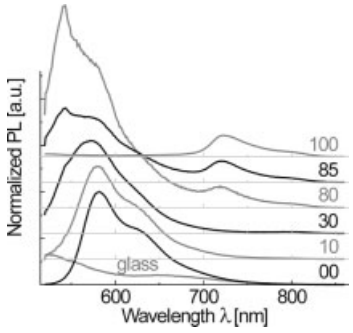

Figure 5. Normalized photoluminescence (PL) spectra of MDMO-PPV/PCBM blends for several compositions (in weight percentage of PCBM) with excitation at 500 nm. 00–30 wt.-% PCBM are normalized at ~580 nm, whereas 80–100 wt.-% PCBM are normalized at ~722 nm. The feature near 543 nm is an artifact of the measurement (see text).

signal must be regarded as a small residual effect. The extremely low signals prevented us from quantifying the amount of PL quenching reproducibly. However, the spectral information can still be used. Up to 30 wt.-% PCBM, a blue-shift of ~10 nm is observed for the emission maximum of MDMO-PPV while at the same time the shoulder at higher wavelengths (~625 nm) disappears. This observation is consistent with the idea that the residual emission originates from increasingly short-lived MDMO-PPV excitations that have not equilibrated. Above 30 wt.-% PCBM, the signal is increasingly contaminated with stray light and Raman effects, as was evidenced by a linear shift of some features with changing excitation wavelength (see, e.g., the narrow peak at ~543 nm in Fig. 5).

PL lifetime measurements can give important additional information on the nature of the blends. Time-correlated single-photon counting PL lifetime measurements have been per-

ADVANCED FUNCTIONAL MATERIALS

formed, probing at characteristic fluorescence wavelengths for MDMO-PPV (584 nm) and PCBM (722 nm) while exciting the samples at 400 nm.

At 584 nm an almost monoexponential fluorescence decay is observed for pure MDMO-PPV (Fig. 6a), corresponding to the lifetime of the singlet excited state. Adding only 2 wt.-% PCBM immediately reduces the observed fluorescence lifetime of MDMO-PPV to the time resolution of the setup (~40 ps)

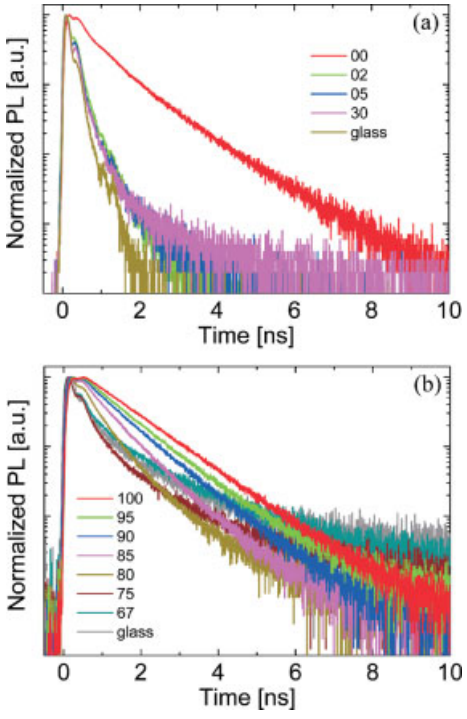

Figure 6. Normalized fluorescence lifetime traces for several MDMO-PPV/PCBM blends with excitation at 400 nm and detection at a) 584 nm, and b) 722 nm. The numbers in the legends refer to the weight percentage of PCBM.

and for higher weight percentage the curves remain almost identical (for clarity only a few are shown in Fig. 6a, together with the signal due to stray light from uncoated glass as a reference). Because photoinduced electron transfer from the polymer to the fullerene is known to occur within ~45 fs,[6] this result indicates that already at 2 wt.-% PCBM virtually all photoexcitations in MDMO-PPV decay via photoinduced charge transfer. This huge effect at such a low concentration of PCBM is only possible when the fullerenes are rather homogeneously distributed over the film, either molecularly or as a large number of small domains. In either case, fullerenes must be present within the exciton diffusion length (~10 nm) of the polymer to explain the strong quenching.

For pure PCBM, the fluorescence at 722 nm of PCBM appears to be monoexponential (Fig. 6b). Upon adding MDMO-PPV to PCBM to bring the PCBM concentration down to 67 wt.-%, the fluorescence lifetime decreases only gradually, in strong contrast to the abrupt changes observed for the MDMO-PPV fluorescence. The gradual reduction in fullerene lifetime with increasing polymer concentration accompanies the decreasing domain size of the PCBM phase observed in AFM and TEM. It should be noted that with decreasing weight percentage of PCBM, the measurement time and therefore the baseline (dark counts) increases. As a result, sensitivity problems of the set-up prevent fluorescence lifetime measurements below 75 wt.-% PCBM.

These results are interpreted by considering that the PCBM domains in the phase-separated composites are rather pure. In such cases, the intrinsic decay of the PCBM singlet excited state (intersystem crossing and fluorescence) competes with hole transfer to the polymer. The fluorescence intensity and lifetime will then critically depend on the balance between the characteristic size of the domains and the exciton diffusion length of the singlet excited state of PCBM. The observed gradual decrease in lifetime can be explained by considering that for increasingly smaller PCBM domains, photoinduced hole transfer from PCBM to MDMO-PPV becomes more likely because excitations created in the PCBM domains will be able to reach the interface with the polymer where they are quenched.

2.5. Device Performance Under Illumination

In the previous paragraphs we have assessed the morphology of MDMO-PPV/PCBM blends using AFM, TEM, and dynamic TOF-SIMS, and obtained additional information on the composition of the two phases from fluorescence experiments. In this section we assess some of the characteristic performance parameters of the solar cells in relation to composition and morphology. For each composition several devices from different preparation batches were made and subsequently measured, both in the dark and under illumination. Typical J–V curves recorded under illumination with filtered white light from a tungsten–halogen lamp[26] are shown in Figure 7a for different compositions. Figures 7b,c show the dependence of the short-circuit current density J_{sc}, open-circuit voltage V_{oc}, fill factor FF,[27] and power conversion efficiency η_{pc}[28] as functions of the weight percentage of PCBM in the blend.[29]

The plot of J_{sc} versus composition (Fig. 7b) reveals that J_{sc} increases gradually with increasing fullerene concentration until it reaches a maximum at 75–80 wt.-%, followed by a rapid decrease.[30] If the PCBM phase related to a random 3D network, the completion of the PCBM electron-transporting phase would be expected at the theoretical percolation threshold of ~17 vol.-%[31] (corresponding to ~25 wt.-% PCBM). However, Figure 7b does not reveal a well-defined percolation threshold for J_{sc}. Instead, the steepest increase in J_{sc} is found in the range of 50–67 wt.-% PCBM, nicely corresponding to the onset of phase separation in the blend as inferred from the AFM and TEM experiments. J_{sc} increases with the further development of the phase separation up to 80 wt.-% PCBM. Beyond 80 wt.-%, the decreasing optical density of the film due to the low absorption cross section of PCBM compared to MDMO-PPV, eventually results in a drop of J_{sc}.

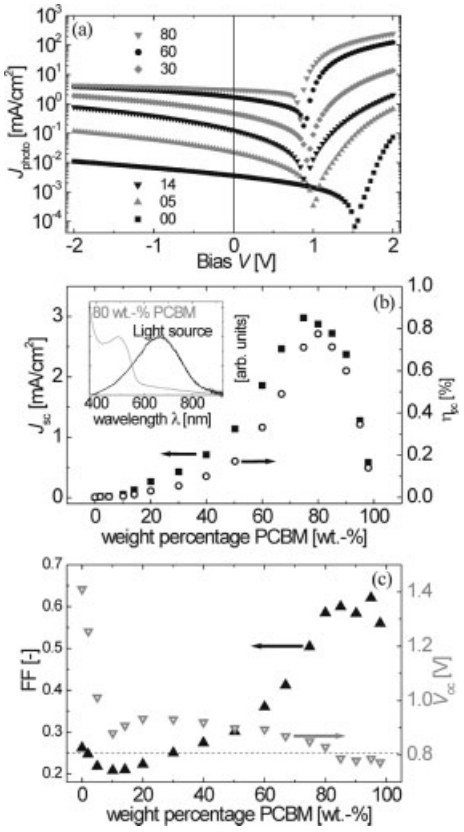

Figure 7. a) Some photocurrents for several weight percentages of PCBM with MDMO-PPV. b) Short-circuit current density (J_{sc}), power conversion efficiency (η_{pc}), c) fill factor (FF), and open-circuit voltage (V_{oc}) with varying composition. Inset in (b) shows spectral overlap between light source used and an 80 wt.-% PCBM film. The dotted line in (c) represents FF = 0.25.

The origin of V_{oc} in these photovoltaic devices is still the subject of some debate.[32] Recent studies by Michailetchi et al. show that in case of ohmic contacts, such as used in this study,[16,33–36] the negative and positive electrodes match the LUMO of the acceptor and the HOMO of the donor, respectively, which govern the V_{oc}.[37] The concentration dependence of V_{oc} (Fig. 7c) is rather different from that of J_{sc}, and seems to be consistent with the proposition made by Michailetchi et al. Already at low concentrations of PCBM in MDMO-PPV, V_{oc} is reduced from the value of 1.4 V for pure MDMO-PPV, to an almost constant value in the range of 0.78–0.95 V (Fig. 7c) for more than 10 wt.-% PCBM (at a light intensity of ~180 mW cm^{-2}).

The evolution of the fill factor as function of the PCBM concentration resembles that of J_{sc}. The overall rise of FF with increasing weight percentage of PCBM indicates a smaller series resistance, and is attributed to more efficient charge transport. The strongest increase in FF is observed between 60 and 75 wt.-%, again corresponding to the range where the phase separation develops. The maximum of $FF = 0.6$ is reached at approximately 80 wt.-% PCBM. Below 50 wt.-%, the FF is extremely low (0.2–0.3), showing that the series resistance (determined by bulk and contact properties) governs the J–V curves, as found for pure MDMO-PPV where both the electrons and holes have a rather low mobility. Between 2 and 30 wt.-% PCBM the FF is actually less than 0.25, which is the theoretical minimum in a single semiconductor photovoltaic model with a large limiting series resistance.[38] It is tempting to relate this phenomenon to an incomplete fullerene electron-transporting network. In contrast to pure MDMO-PPV, photogenerated electrons in blends are mainly localized on PCBM molecules. When the fullerene network is incomplete as a result of a low amount of fullerenes, electron transport is hindered and likely to be strongly field-dependent. As a result, the recombination of photogenerated charges will be extremely large and J_{sc} low. Going from V_{oc} to 0 V (J_{sc}), transport will be enhanced by the increasing electric field (which is zero at V_{oc}), resulting in a bending of the J–V curve in the wrong direction (FF < 0.25).

The change in power conversion efficiency η_{pc} (Fig. 7b) with varying composition is of course a straightforward combination of the changes in J_{sc}, V_{oc}, and FF, and confirms that the cells reach a maximum performance at 80 wt.-% PCBM.[9] It is important to note that the absolute values for η_{pc} in Figure 7b are not related to standard solar light (AM 1.5) conditions because a filtered tungsten–halogen lamp was used instead of a calibrated solar simulator.[39] Based on the maximum incident photon to current conversion efficiency (IPCE), V_{oc}, and FF however, we conclude that our devices have a similar performance as those published by Shaheen et al.[9]

2.6. Incident-Light Power Dependence

To gain a further insight in the operation of the devices, J_{sc}, V_{oc}, and FF have been studied as function of incident-light intensity (Fig. 8).

The short-circuit current density was found to increase with incident light power (ILP) according to a power-law behavior $J_{sc} \propto \mathrm{ILP}^{\alpha}$. For compositions in the range of 67–90 wt.-% PCBM, the power-law exponent α equals 0.94,[40] consistent with previous results.[41] The slightly sublinear dependence suggests some bimolecular recombination of positive and negative photogenerated charges. For blends with less than 67 wt.-% PCBM, α gradually decreases to 0.71 at 10 wt.-%. We attribute this reduction to an increased bimolecular recombination. Because phase separation is not observed below 67 wt.-%, charge recombination is stronger in the homogenous MDMO-PPV/PCBM phase.

Most samples show an onset of V_{oc} at ILP $\approx 10^{-2}$ mW cm^{-2}, where the sharp increase in V_{oc} with ILP is followed by a less steep increase above ~1 mW cm^{-2} (see Fig. 8, for clarity only a few curves are shown). The onset of V_{oc} with ILP is strongly related to the film thickness. For films with 80 wt.-% PCBM, the onset at 10^{-2} mW cm^{-2} decreases to 10^{-4} mW cm^{-2} when the thickness of the film is increased from 110 to 170 nm. Compared to the blends, the onset of V_{oc} for devices prepared using (almost) pure materials (0, 3, and 90 wt.-%) occurs at much higher light intensities (10^{-1} –1 mW cm^{-2}). The onset of V_{oc} is determined by the minimum amount of photogenerated charges present in the bulk necessary to oppose the applied

ADVANCED FUNCTIONAL MATERIALS

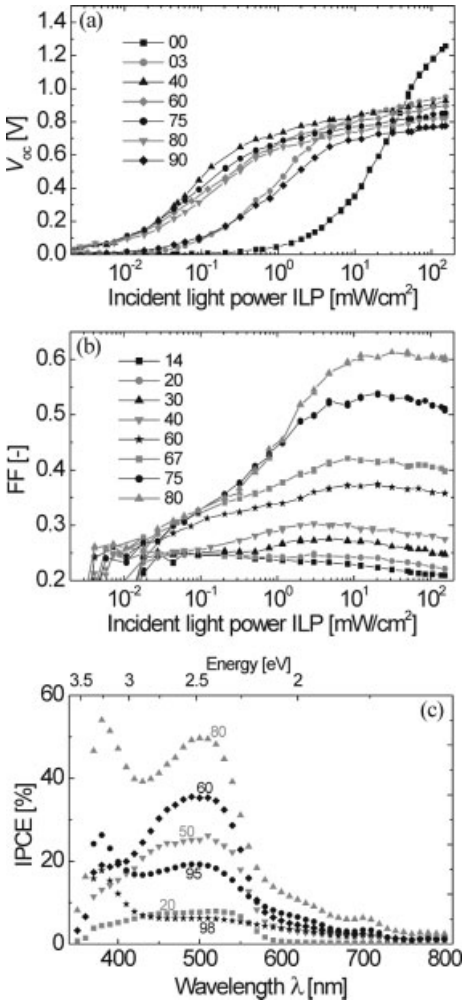

Figure 8. V_{oc} (a) and FF (b) with varying incident light power (ILP) for several compositions (in weight percentage of PCBM). c) Incident photon to current conversion efficiency (IPCE) spectra for some compositions.

electric field. Therefore, the dependence on film thickness (optical density) and composition (i.e., charge generation efficiency) seem straightforward. The fill factor also shows an onset at ILP $\approx 10^{-2}$ mW cm^{-2} but then goes through a maximum value, followed by a small decrease (Fig. 8). With increasing weight percentage of PCBM the maximum of FF is observed for higher ILP. The fact that the FF is only slightly decreasing with ILP demonstrates that charge recombination in MDMO-PPV/PCBM devices at high light intensities is not as strong as in other blend systems.[42]

2.7. Wavelength Dependence (IPCE)

The incident photon to current conversion efficiency (IPCE,[43] Fig. 8) for a range of compositions reveals that light absorbed by either MDMO-PPV or PCBM contributes to the photocurrent. This is in accordance with recent photophysical data, showing that both excitation of the polymer and the fullerene result in a sub-picosecond charge separation.[4] In the graphs, the contribution of PCBM to the photocurrent can be easily recognized above 580 nm, with a highly characteristic peak of the lowest singlet excited state of PCBM at 705 nm,[44] while the MDMO-PPV absorption is evident from the peak at 500 nm. Hence, there is no doubt that for these composite devices the contribution of both photoinduced electron and hole transfer play a significant role. Remarkably, the characteristic signatures of PCBM in the IPCE spectra below 400 nm and at 705 nm become more pronounced above 60 wt.-%. However, unraveling the quantitative contributions of MDMO-PPV and PCBM to the IPCE spectra needs further investigation, where the influence of different charge transfer efficiencies, waveguiding effects, space–charge-distribution, and a possible charge-generation depth profile have to be taken into consideration.

2.8. Dark *J–V* Curves

Previously it has been shown that the dark current in pure MDMO-PPV and PCBM is space-charge limited under forward bias, when the materials are sandwiched between ohmic PEDOT–PSS and LiF/Al contacts, as used in this study. Because the mobility of the holes in pure MDMO-PPV[45] is 4000 times less than the electron mobility in pure PCBM,[16] it is of interest to study the *J–V* characteristics in the dark and see whether it is possible to relate the changes in the dark current with varying composition to the formation of a fullerene electron-transporting network and to possibly identify a percolation threshold.

The measured dark currents are shown in Figure 9. On the horizontal axis the applied voltage is shown, corrected for the built-in voltage V_{bi} (which was taken as the compensation voltage V_0[46–49]) and for the voltage drop (V_{RS}) over the contacts.[50] Because space–charge-limited current (SCLC) strongly depends on film thickness ($J_{SCLC} \propto L^{-3}$), the values of J_{dark} in

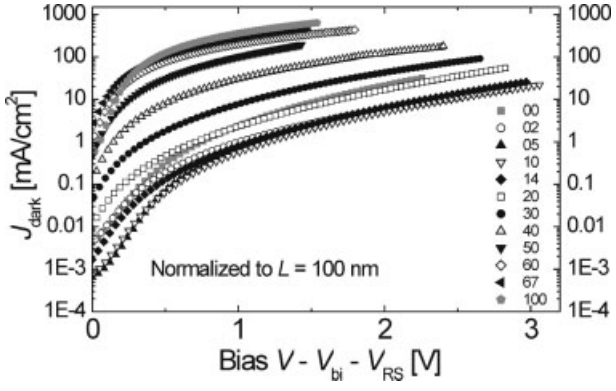

Figure 9. Dark current densities (J_{dark}) for varying weight percentages of PCBM blends with MDMO-PPV, normalized to 100 nm thickness according to SCLC ($J_{dark} \propto L^{-3}$) as function of the applied bias after correction for the built-in voltage V_{bi} and the voltage drop (V_{RS}) over the contacts (see text).

Figure 9 have been corrected for the small variations in film thickness (normalized at 100 nm). At values of $V - V_{bi} - V_{RS} > 1$, J_{dark} scales approximately with $(V - V_{bi} - V_{RS})^2$ as expected for SCLC behavior. Figure 9 shows that from 2 wt.-% PCBM the dark current drops below that of the hole-governed device of MDMO-PPV and becomes minimal at 5–10 wt.-% PCBM. Subsequently, the dark current strongly increases and saturates at approximately 67 wt.-% PCBM. With increasing fullerene concentration the electron transport starts to dominate the dark current in these devices. The saturation behavior at 67 wt.-% seems closely related to the transition from one to two phases as observed with AFM and TEM and coincides with the composition where the exponent α in $J_{sc} \propto \mathrm{ILP}^{\alpha}$ becomes maximal.

Continuous percolation pathways from bottom to top electrode for both p- and n-type semiconductors in thin-film bulk-heterojunction diodes result in an increased conductivity compared to bilayer or stratified structures. In accordance, also the current in reverse bias increases with increasing weight percentage of PCBM typically from 10^{-3}–10^{-2} mA cm^{-2} at –2 V (reverse bias) for 0–40 wt.-% to 0.1 mA cm^{-2} for 60–90 wt.-% with again a clear transition at the concentration where phase separation starts to set in. An additional step from 0.1 mA cm^{-2} for 60–90 wt.-% to 1 mA cm^{-2} for 95–100 wt.-% PCBM can be observed. This last increase is mainly attributed to shunting due to a decrease in film quality for these highly phase separated films.

3. Conclusions

We have shown by AFM and TEM that for ~100 nm composite MDMO-PPV/PCBM films, spin-cast from chlorobenzene, nanoscale phase separation sets in at approximately 67 wt.-% PCBM. The phase separation gives rise to almost pure PCBM domains in a surrounding matrix of MDMO-PPV that contains up to 50 wt.-% PCBM. TEM and AFM measurements at the bottom of sputtered craters have shown that this lateral phase separation is present at all depths and dynamic TOF-SIMS has confirmed the absence of a spontaneous stratification in the vertical direction. Additionally, time-correlated single-photon-counting fluorescence measurements revealed that up to 50 wt.-% PCBM the fullerenes are homogeneously distributed over the film either molecularly or in the form of tiny domains.

Electrical characterization of the composite photovoltaic devices, both in the dark and under illumination (J_{sc}, V_{oc}, and FF), reveals that in the range of 50–75 wt.-% PCBM, where phase separation sets in, a dramatic increase in J_{sc} and FF occurs. In accordance, the exponent α in $J_{sc} \propto \mathrm{ILP}^{\alpha}$ and the dark currents in forward bias start to saturate above 67 wt.-% PCBM, with a clear increase in the shunting as observed in reverse bias. As a consequence of the increased charge transport and collection efficiency, less recombination occurs with increasing fullerene concentration. The open-circuit voltage is much less dependent on the concentration as it seems to be related to the nature of the components and less to the morphology.

The results described above point to an intricate relation between the morphology and device performance. The virtually homogeneous blend that is present up to 50 wt.-% PCBM represents without much doubt, a perfect morphology for very efficient charge generation. The PL lifetime experiments have shown that virtually every excitation created in this phase on either MDMO-PPV or PCBM is quenched and, hence, provides charges. The fact that, more (80 wt.-%) PCBM is necessary to have the optimum performance of the solar cell, must therefore be due to the fact that not all photogenerated charges can be collected at the electrodes and recombine, either geminately or non-geminately. At 67 wt.-% PCBM, nanoscale phase separation sets in, which apparently reduces recombination. One could envision that a negative charge injected into a pure PCBM phase delocalizes and does not easily recombine with the hole left in the polymer matrix. The fact that 80 wt.-% is the optimum, can be rationalized by considering that also the pure PCBM phase must build a percolating network with pathways large enough in size to facilitate escape from the interface, which it can only do starting from 67 wt.-%. In that sense, one could think of a hierarchical build up of two cooperative interpenetrating networks on different length scales. The first one is a percolating network of molecularly dispersed fullerenes (or tiny clusters thereof) in the 50 wt.-% PCBM homogenous matrix, and the second one is a percolating network of a dimension that is one order of magnitude larger and consists of pure PCBM domains or nanocrystals. Such a fractal-like combination of percolating PCBM networks, bears similarities to the vascular system consisting of a capillary system and arterioles.

The combination of MDMO-PPV, PCBM, chlorobenzene, substrate, and casting conditions results in an optimum of 80 wt.-% PCBM. Of course, for other materials and processing conditions the morphology and optimum might be completely different, but the necessity of both continuous percolating pathways and a minimum domain size to facilitate escape from the interface and overcome excessive recombination losses will certainly prove to be general for other systems as well. This systematic study provides the opportunity to speed up optimization work of bulk-heterojunction solar-cell performance for a combination of two new materials by extraction of morphological issues from the device characteristics.

4. Experimental

Materials: Materials used were MDMO-PPV [51], PCBM, poly(ethylenedioxythiophene)–poly(styrenesulfonate) (PEDOT–PSS) (Baytron P VPAI 4083), LiF (Aldrich), and Al (Engelhard-Clal). MDMO-PPV has $M_w \approx 1 \times 10^6$ g mol^{-1} and a polydispersity of about 7 as determined by size exclusion chromatography (SEC), calibrated against polystyrene. The glass-transition temperature $T_g = 80$ °C of MDMO-PPV was measured with dynamic mechanical thermal analysis (DMTA). The synthesis of d5-PCBM was similar to that of PCBM and details will be reported elsewhere. A glass substrate covered with indium tin oxide

ADVANCED FUNCTIONAL MATERIALS

(ITO) (40 nm) was used as the substrate for AFM, TEM, and dynamic TOF-SIMS. Glass plates covered with 160 nm patterned ITO resulting in four different device areas (0.1, 0.15, 0.33, 1.0 cm^2) were used for devices. Schott D263 glass plates were used for spectroscopic investigations.

Device Preparation: Cleaned [24] ITO-covered glass substrates were covered with a ~100 nm PEDOT–PSS layer by spin coating, dried for 1 min at 180 °C, and then cooled for 1 min at 25 °C. Composite layers of 80–130 nm MDMO-PPV and PCBM (thickness variation between compositions) were spin-coated from chlorobenzene solution and the samples were transferred to a N_2 atmosphere glove box. Finally, ~10 Å LiF and ~110 nm Al layers were deposited by thermal evaporation in vacuum (5×10^{-6} mbar, 1 ppm O_2 and < 1 ppm H_2O) with the samples 1–2 h in vacuum before evaporation. The samples were rotated at ~1 Hz during deposition to guarantee homogeneous films. The organic solutions are stirred vigorously overnight while keeping them in the dark. Film thickness for the different composite samples was controlled by reducing the concentration of the composite solution from 5.4 to 0.5 mg MDMO-PPV per milliliter of chlorobenzene with increasing weight percentage of PCBM. It should be noted that the variation in film thickness between substrates per composition is below 4 nm, whereas the film thickness varies randomly going from 0–100 wt.-% PCBM. The same procedure was used to prepare samples for morphological and spectroscopic studies with 70–115 nm composite layers on ~75 nm PEDOT–PSS for the morphological studies. All samples were stored in the dark in an N_2 atmosphere glove box. Film thickness measurements were performed with a Tencor P10 surface profiler.

Device Measurements: All measurements were performed in a N_2 atmosphere at room temperature. In forward bias the ITO electrode was positively biased. *J–V* characteristics were measured with a Keithley 2400 source meter. For white light illumination (~180 mW cm^{-2}) a tungsten–halogen lamp was used, filtered by a Schott KG1 and GG385 filter resulting in a spectral range of 400–900 nm with its maximum at ~650 nm. Light power is measured with an Ophir Laser Power Meter set at 610 nm. Incident light power was varied over five orders of magnitude with a series of metal-coated neutral density filters. Spectrally resolved photocurrents were measured using monochromatic light (~0.03 mW cm^{-2}), calibrated against a multicrystalline (mc) Si solar cell with a known spectral response. The stability of the devices was found to be more than sufficient to perform all the above measurements.

Atomic Force Microscopy: A solver P47H atomic force microscope (NT-MDT Co., Moscow, Russia) in resonant (alternating current (AC) or tapping) mode was used to measure height and phase images with both NT-MDT NSG01 (force constant is typically 5.5 N m^{-1}) and NSG10 (force constant is typically 11.5 N m^{-1}) cantilevers.

Transmission Electron Microscopy (TEM): Film preparation for TEM is described above under device preparation. Two methods were used to prepare the TEM specimen. One is mechanically removing from its substrate with adhesive tape. The other one is the floatation technique by using deionized water. The films were floated onto the surface of deionized water and finally picked up by a 400 mesh copper grid. The TEM observations were conducted on a JEOL JEM-2000FX transmission electron microscope operated at 80 kV.

Dynamic TOF-SIMS: The dynamic SIMS measurements were performed on an ION-TOF TOF-SIMS IV apparatus (which saturates at 3×10^5 counts) in dual-beam mode: 73 nA 1 keV Cs^+ at 45° rastered over 300 μm × 300 μm for sputtering and a 15 keV Ga^+ beam (1.9, 2.5, and 3.0 pA) at 45° rastered over 50 μm × 50 μm for analysis. The depth profiles were measured in the non-interlaced mode (longer sputter and data acquisition cycles) to avoid charging. Effective charge compensation was obtained by using an electron flood gun (20 eV). All depth profiles were taken in the negative mode and mass calibrated on C_xH_y fragments.

Absorption and Fluorescence Spectroscopy: Absorption spectra were recorded on a Perkin-Elmer Lambda 900 spectrophotometer. Fluorescence spectra were recorded on an Edinburgh Instruments FS920 double-monochromator spectrometer with a Peltier-cooled red-sensitive photomultiplier. Depending on the spectral range, appropriate cut-off filters were inserted in the excitation beam. Time-correlated single-photon-counting fluorescence studies were performed using an Edinburgh Instruments LifeSpec-PS spectrometer, consisting of a 400 nm picosecond laser (PicoQuant PDL 800B) operated at 2.5 MHz and a Peltier-cooled Hamamatsu micro-channel plate photomultiplier (R3809U-50), where appropriate cutoff filters were put in the detection beam.

Received: September 19, 2003
Final version: November 19, 2003

[1] G. Yu, J. Gao, J. C. Hummelen, F. Wudl, A. J. Heeger, *Science* **1995**, *270*, 1789.
[2] J. J. M. Halls, C. A. Walsh, N. C. Greenham, E. A. Marseglia, R. H. Friend, S. C. Moratti, A. B. Holmes, *Nature* **1995**, *376*, 498.
[3] P. Schilinsky, C. Waldauf, and C. J. Brabec, *Appl. Phys. Lett.* **2002**, *81*, 3885.
[4] M. M. Wienk, J. M. Kroon, W. J. H. Verhees, J. Knol, J. C. Hummelen, P. A. van Hal, R. A. J. Janssen, *Angew. Chem. Int. Ed.* **2003**, *42*, 3371.
[5] N. S. Sariciftci, L. Smilowitz, A. J. Heeger, F. Wudl, *Science* **1992**, *258*, 1474.
[6] C. J. Brabec, G. Zerza, G. Cerullo, S. De Silvestri, S. Luzzati, J. C. Hummelen, N. S. Sariciftci, *Chem. Phys. Lett.* **2001**, *340*, 232.
[7] I. Montanari, A. F. Nogueira, J. Nelson, J. R. Durrant, C. Winder, M. A. Loi, N. S. Sariciftci, C. J. Brabec, *Appl. Phys. Lett.* **2002**, *81*, 3001.
[8] T. Offermans, S. C. J. Meskers, R. A. J. Janssen, *J. Chem. Phys.* **2003**, *119*, 10 467.
[9] S. E. Shaheen, C. J. Brabec, N. S. Sariciftci, F. Padinger, T. Fromherz, J. C. Hummelen, *Appl. Phys. Lett.* **2001**, *78*, 841.
[10] J. Liu, Y. Shi, Y. Yang, *Adv. Funct. Mater.* **2001**, *11*, 420.
[11] N. Camaioni, G. Ridolfi, G. Casalbore-Miceli, G. Possamai, M. Maggini, *Adv. Mater.* **2002**, *14*, 1735.
[12] F. Padinger, R. S. Rittberger, N. S. Sariciftci, *Adv. Funct. Mater.* **2003**, *13*, 85.
[13] T. Martens, J. D'Haen, T. Munters, Z. Beelen, L. Goris, J. Manca, M. D'Olieslaeger, D. Vanderzande, L. De Schepper, R. Andriessen, *Synth. Met.* **2003**, *138*, 243.
[14] A. C. Arias, J. D. MacKenzie, R. Stevenson, J. J. M. Halls, M. Inbasekaran, E. P. Woo, D. Richards, R. H. Friend, *Macromolecules* **2001**, *34*, 6005.
[15] H. J. Snaith, A. C. Arias, A. C. Morteani, C. Silva, R. H. Friend, *Nano Lett.* **2002**, *2*, 1353.
[16] V. D. Mihailetchi, J. K. J. van Duren, P. W. M. Blom, J. C. Hummelen, R. A. J. Janssen, J. M. Kroon, M. T. Rispens, W. J. H. Verhees, M. M. Wienk, *Adv. Funct. Mater.* **2003**, *13*, 43.
[17] C. W. T. Bulle-Lieuwma, W. J. H. van Gennip, J. K. J. van Duren, P. Jonkheijm, R. A. J. Janssen, J. W. Niemantsverdriet, *Appl. Surf. Sci.* **2003**, *203–204*, 547.
[18] K. A. Welp, R. P. Wool, S. K. Satija, S. Pispas, J. Mays, *Macromolecules* **1998**, *31*, 4915.
[19] H. Yokoyama, E. J. Kramer, M. H. Rafailovich, J. Sokolov, S. A. Schwarz, *Macromolecules* **1998**, *31*, 8826.
[20] S. J. Valenty, J. J. Chera, D. R. Olson, K. K. Webb, G. A. Smith, W. Katz, *J. Am. Chem. Soc.* **1984**, *106*, 6155.
[21] P. C. Zalm, *Mikrochim. Acta* **2000**, *132*, 243.
[22] It should be noted that with increasing polymer concentration the overlap in mass between the isotope clusters $^{13}C^1H$ with $^{12}C^2H$ (= CD), and $^1H_2$ with ^2H (= D) results in an increasing contribution of the non-deuterium related isotopes to the ion yields of CD, CHD, and C_2D from < 10 % for 100 wt.-% d5-PCBM to ~30 % at 40 wt.-% d5-PCBM, as can be concluded from comparison with the undeuterated composites.
[23] L. Chen, D. Godovski, O. Inganäs, J. C. Hummelen, R. A. J. Janssen, M. Svensson, M. R. Andersson, *Adv. Mater.* **2000**, *12*, 1367.

[24] J. K. J. van Duren, J. Loos, F. Morrisey, C. M. Leewis, K. P. H. Kivits, L. J. van IJzendoorn, M. T. Rispens, J. C. Hummelen, R. A. J. Janssen, *Adv. Funct. Mater.* **2002**, *12*, 665.

[25] T. J. Savenije, J. E. Kroeze, M. M. Wienk, J. M. Kroon, J. M. Warman, unpublished.

[26] The spectral overlap between the light source and the absorption spectrum of the 80 wt.-% PCBM film is shown in the inset of Figure 7b.

[27] The fill factor is defined as: $FF = (J_{max}V_{max})/(J_{sc}V_{oc})$ where J_{max} and V_{max} are current density and voltage at the maximum power point, respectively.

[28] The power conversion efficiency is defined as $\eta_{pc}[\%] = (J_{sc}V_{oc}\times FF)/ILP$ with ILP the incident light power.

[29] The standard deviation of the short-circuit current density (J_{sc}) and power conversion efficiency (η_{pc}) is below 10 % of the average. The light source has a deviation of 3 % in light power. The open-circuit voltage (V_{oc}) has a standard deviation of ~1 % for every composition, except for the pure MDMO-PPV and 2 wt.-% PCBM devices whose standard deviation for V_{oc} is somewhat larger (~7 %). The V_{oc} for these low fullerene concentrations is very sensitive to film thickness and shorts density as a result of the photocurrent and leakage current being of the same order of magnitude. The fill factor (FF) has a standard deviation of ~1 % for every composition.

[30] Due to poor film-forming properties of pure PCBM, the ~100 nm spin-cast films contain tiny holes (as observed with AFM) making reproducibility of the solar cell results poor and the influence of leakage current extremely large. Therefore, no data of photocurrents coming from pure PCBM are included.

[31] M. Sahimi, *Applications of Percolation Theory*, Taylor & Francis, London **1994**.

[32] C. J. Brabec, A. Cravino, D. Meissner, N. S. Sariciftci, T. Fromherz, M. T. Rispens, L. Sanchez, J. C. Hummelen, *Adv. Funct. Mater.* **2001**, *11*, 374.

[33] T. M. Brown, F. Cacialli, *J. Polym. Sci., Part B: Polym. Phys.* **2003**, *41*, 2649.

[34] T. M. Brown, R. H. Friend, I. S. Millard, D. J. Lacey, T. Butler, J. H. Burroughes, F. Cacialli, *J. Appl. Phys.* **2003**, *93*, 6159.

[35] M. Fahlman, W. R. Salaneck, *Surf. Sci.* **2002**, *500*, 904.

[36] The work functions for PEDOT–PSS (5.2 eV) and LiF/Al (~3.7 eV), match with the HOMO level of MDMO-PPV (5.3 ± 0.1 eV) and the LUMO level of PCBM (3.7 eV), see reference [37].

[37] V. D. Michailetchi, P. W. M. Blom, J. C. Hummelen, M. T. Rispens, *J. Appl. Phys.* **2003**, *94*, 6849.

[38] A. L. Fahrenbruch, R. H. Bube, *Fundamentals of Solar Cells*, Academic Press, New York **1983**.

[39] J. M. Kroon, M. M. Wienk, W. J. H. Verhees, J. C. Hummelen, *Thin Solid Films* **2002**, *403–404*, 223.

[40] Fitting is performed over the upper part of the measured range (three orders of magnitude, $R > 0.999$) where both V_{oc} and FF are clearly beyond their threshold value. When fitted over the full range (five orders of magnitude) the trend in the slope with varying composition is unaffected, but statistics deteriorate.

[41] V. Dyakonov, I. Riedel, C. Deibel, J. Parisi, C. J. Brabec, N. S. Sariciftci, J. C. Hummelen, *Mater. Res. Soc. Symp. Proc.* **2002**, *665*, 235.

[42] W. U. Huynh, J. J. Dittmer, A. P. Alivisatos, *Science* **2002**, *295*, 4510.

[43] The incident photon to current conversion efficiency (or external quantum efficiency) is defined as: $IPCE\ [\%] = (1.24\times10^5\times J_{sc})/(ILP\times\lambda)$ with J_{sc} [mA cm^{-2}], ILP [mW cm^{-2}], and λ [nm] the wavelength of the monochromatic light.

[44] R. A. J. Janssen, J. C. Hummelen, F. Wudl, *J. Am. Chem. Soc.* **1995**, *117*, 544.

[45] P. W. M. Blom, M. J. M. de Jong, M. G. van Munster, *Phys Rev B.: Condens. Matter Mater. Phys.* **1997**, *55*, R656.

[46] G. G. Malliaras, J. R. Salem, P. J. Brock, J. C. Scott, *J. Appl. Phys.* **1998**, *84*, 1583.

[47] X. Wei, M. Raikh, Z. V. Vardeny, Y. Yang, D. Moses, *Phys. Rev. B: Condens. Matter Mater. Phys.* **1994**, *49*, 17 480.

[48] H. Frohne, S. E. Shaheen, C. J. Brabec, D. C. Müller, N. S. Sariciftci, K. Meerholz, *ChemPhysChem* **2002**, *3*, 795.

[49] $V_0 \approx V_{oc} + 0.2$ V for 0 and 2 wt.-%, whereas $V_0 \approx V_{oc} + 0.05$ V for all other concentrations.

[50] For current densities larger than 100 mA cm^{-2}, the applied voltage should be corrected for the voltage drop across the indium tin oxide (ITO) series resistance V_{RS}, which typically amounts to 25 Ω in our substrates.

[51] H. Becker, H. Spreitzer, W. Kreuder, E. Kluge, H. Schenk, I. Parker, Y. Cao, *Adv. Mater.* **2000**, *12*, 42.

